Article

Manipulation of Microstructure and Mechanical Properties in N-Doped CoCrFeMnNi High-Entropy Alloys

Jing Zhang [1,2], **Kook Noh Yoon** [2], **Min Seok Kim** [2], **Heh Sang Ahn** [2], **Ji Young Kim** [2], **Wook Ha Ryu** [2] **and Eun Soo Park** [2,*]

1   School of Metallurgy and Materials Engineering, Jiangsu University of Science and Technology, Zhangjiagang 215600, China; sduzhangjing@126.com
2   Department of Materials Science and Engineering, Research Institute of Advanced Materials & Institute of Engineering Research, Seoul National University, Seoul 08826, Korea; ykn2002@snu.ac.kr (K.N.Y.); ivy94@snu.ac.kr (M.S.K.); ahs1012@snu.ac.kr (H.S.A.); kzy94@snu.ac.kr (J.Y.K.); ldsruh@snu.ac.kr (W.H.R.)
*   Correspondence: espark@snu.ac.kr

Abstract: Herein, we carefully investigate the effect of nitrogen doping in the equiatomic CoCrFeMnNi high-entropy alloy (HEA) on the microstructure evolution and mechanical properties. After homogenization (1100 °C for 20 h), cold-rolling (reduction ratio of 60%) and subsequent annealing (800 °C for 1 h), a unique complex heterogeneous microstructure consisting of fine recrystallized grains, large non-recrystallized grains, and nanoscale Cr_2N precipitates, were obtained in nitrogen-doped (0.3 wt.%) CoCrFeMnNi HEA. The yield strength and ultimate tensile strength can be significantly improved in nitrogen-doped (0.3 wt.%) CoCrFeMnNi HEA with a complex heterogeneous microstructure, which shows more than two times higher than those compared to CoCrFeMnNi HEA under the identical process condition. It is achieved by the simultaneous operation of various strengthening mechanisms from the complex heterogeneous microstructure. Although it still has not solved the problem of ductility reduction, as the strength increases because the microstructure optimization is not yet complete, it is expected that precise control of the unique complex heterogeneous structure in nitrogen-doped CoCrFeMnNi HEA can open a new era in overcoming the strength–ductility trade-off, one of the oldest dilemmas of structural materials.

Keywords: high-entropy alloy; nitrogen doping; heterogeneous microstructure; strengthening; strength–ductility trade-off

1. Introduction

The single-phase FCC CoCrFeMnNi high-entropy alloy (HEA) has potential advantages in hardness, toughness, thermal stability, and excellent plasticity at room temperature and low temperature [1–5]. For example, at 293 K, the elongation of CoCrFeMnNi HEA can reach 80% [6]. Furthermore, the ductile–brittle transition will not occur even at 15 K, and the elongation can remain about 60% [7,8]. Therefore, the CoCrFeMnNi HEA has an important engineering application prospect in structural materials, especially in the cryogenic field. However, the strength of the CoCrFeMnNi HEA is not high enough, especially at room temperature. The yield strength of CoCrFeMnNi HEA (with a large grain size of 155 μm) is only 125 MPa [6], which severely limits its engineering application. Thus, the strengthening of CoCrFeMnNi HEA is an urgent issue to be solved as the key material property. Indeed, there are a lot of efforts to improve the strength of the CoCrFeMnNi HEA by using various strengthening mechanisms through precise control of the microstructure [9–13].

The interstitial solid solution strengthening can introduce a larger lattice distortion in HEA because of the large atomic size mismatch between the interstitial atoms and other constituting elements. Therefore, the strengthening effect is significantly greater than that of the substitutional solid solution. Moreover, the addition of interstitial atoms is very cost-effective because a small amount of addition (below several wt.%) results in an

excellent strengthening effect. Finally, the adjustment of the post-processing conditions, which generate heterogeneous microstructure, can be used to obtain the synergetic effect of various strengthening mechanisms [14–18].

The common reinforcement elements of the interstitial solid solution are carbon, boron, nitrogen, and oxygen. Among the interstitial atoms, nitrogen (N) is widely used in commercial alloys because of its high solid-solution strengthening coefficient and low cost. Therefore, N-doping can enhance the mechanical properties and reduce the production cost of the alloys, such as in the case of stainless steel. Moreover, N can improve the corrosion resistance, leading to high-N steel being studied widely in various commercial steels. Recently, Xie et al. [19] reported the compressive yield strength of CoCrFeMnNi HEA with 0.1 wt.% N increased by 200 MPa, while the elongation was only reduced by 3.4%, which means a small amount of N addition in CoCrFeMnNi HEA is very effective to improve strength without severe reduction of ductility. Furthermore, Klimova et al. [20] reported the yield strength of the as-cast CoCrFeMnNi HEAs with different N contents (nominal 0.5~2.0 at.%) increased in proportion to the percentage of N by 117 MPa/at% N at 293 K, which means that the HEAs with a higher N content exhibit higher strength and better strain-hardening capacity. Jodi et al. [21] added much higher N contents up to 0.95 wt.% to CoCrFeMnNi HEA. After rolling and recrystallization at low temperatures, ultra-fine grains with uniformly distributed Cr_2N were obtained. Compared to CoCrFeMnNi HEA with the same process, the tensile yield strength was increased by about 57 MPa, while the plasticity did not decrease significantly. Eventually, Xiong et al. [22] reported more systematic influences of nitrogen alloying on microstructural evolution and tensile properties of CoCrFeMnNi HEA treated by cold-rolling and subsequent annealing at different annealing temperatures (773–1173 K). However, most research, until now, on N-doped HEA is mainly focused on controlling the parameters to obtain homogeneous microstructure. Despite this trend, introducing heterogeneity in the microstructure (such as gradient, harmonic, layered, bimodal, hierarchical nanostructure, etc. [23–29]) is another promising strategy to improve the HEA's strength.

The strengthening of heterogeneous microstructure in single-phase FCC HEA is mainly achieved by adjusting the recrystallization temperature after rolling deformation. Bae et al. [30] obtained heterogeneous microstructure with irregular grain sizes by tempering at medium annealing temperature (650 °C for 1 h) after cold-rolling. The strength of the CoCrFeMnNi HEA was increased to 625 MPa, and the elongation remained at around 50%. Wu et al. [31] systematically studied the relationship between the hardening mechanism and the heterogeneous microstructure in different strain conditions by the sequence of loading–unloading–reloading, using an insitu tensile test under the electron microscope. The results show that the high yield strength of HEA with heterogeneous microstructure is due to the huge back stress inside. Moreover, the excellent processing hardening ability is because of the plastic deformation which stimulates multi-processing hardening mechanisms, such as back stress strengthening, twin strengthening, and dislocation strengthening. On the other hand, recent research shows that interstitial atoms such as carbon and nitrogen can inhibit the recrystallization process and form heterogeneous microstructure by the interaction between recrystallization and precipitation [32]. For example, Semenyuk et al. [33] reported an increase in the N content hindered the development of recrystallization processes in CoCrFeMnNi HEA. Thus, in the HEA with nominal 2.0 at.% N, a 100% non-recrystallized microstructure was obtained in the condition of annealing at 700 °C for 1 h, while 69% recrystallized microstructure was obtained in the condition of annealing at 800 °C for 1 h. However, to optimize the strengthening effect, a more in-depth study on how complex heterogeneous microstructures are formed through competition between recrystallization and precipitation according to the N contents and/or post-processing conditions and the strengthening effect caused by each structural difference is necessary.

In the present study, we carefully investigated the effect of nitrogen doping on the microstructure evolution and mechanical properties by comparing equiatomic CoCrFeMnNi HEA and N-doped (0.3 wt.%) CoCrFeMnNi HEA. To form the complex heterogeneous

microstructure in N-doped HEA, the HEAs were processed by cold-rolling (reduction ratio of 60%) and subsequent annealing (800 °C for 1 h) after homogenization (1100 °C for 20 h). Finally, the strengthening behavior of the N-doped HEA with complex heterogeneous microstructure compared to CoCrFeMnNi HEA under the identical post-processing condition was carefully discussed based on intensive structural analysis.

2. Experimental

The equiatomic CoCrFeMnNi HEAs is nominally composed of 20 at.% cobalt, 20 at.% chromium, 20 at.% iron, 20 at.% nickel, and 20 at.% manganese. The Fe_4N compound powder is used as the source of nitrogen for the N-doped CoCrFeMnNi HEA. Both HEAs (CoCrFeMnNi HEA and N-doped (0.3 wt.%) CoCrFeMnNi HEA) were prepared by arc-melting a mixture of pure metals (purity higher than 99.95%) and Fe_4N compound powder depending on N contents and re-melted at least five times to promote the chemical homogeneity in a Ti-gettered high-purity argon atmosphere. The molten alloy was cast into a water-cooled copper mold to form a plate with a length of 50 mm, a width of 16 mm, and a thickness of 6 mm. The as-cast samples were homogenized at 1100 °C for 20 h, followed by water quenching. Moreover, a cold-rolling process with 60% thickness reduction at room temperature was conducted (named after as-rolled HEA), subsequently followed by annealing at 800 °C for 1 h (named after as-annealed HEA).

Oxygen and nitrogen analyzer (Flash 2000, Thermo Fisher Scientific, Waltham, MA, USA) were used to determine the nitrogen content after the homogenization process. The measured N-content in N-doped CoCrFeMnNi HEA was 0.3 wt.%. Therefore, the CoCrFeMnNi HEA without and with nitrogen in this study are abbreviated as N0 and N0.3 HEA.

The crystal structures of HEAs were obtained from X-ray diffraction (XRD, Bruker D2 Phaser diffractometer) with the Cu-Kα radiation at 30 kV. The wavelength of the applied X-ray was 1.54056 Å. The XRD curves were measured with straining in the angular range from 30 to 100 deg (2θ) with a step size of 0.01 and a counting time of 2 s per step. The microstructure of the samples was observed by field-emission scanning electron microscope (FE-SEM, Tescan Mira3, Burno, Czech) equipped with electron backscatter diffraction (EBSD, Bruker e-Flash, Karlsruhe, Germany) and energy-dispersive spectrometer(EDS, Bruker xFlash 6130, Karlsruhe, Germany). The EBSD scan step size was 75 nm and a tolerance angle of 15° was used for grain identification. The grain size, calculated with the average values of grain size, using intercept or planimetric methods [34], was measured by Esprit 2.1 software (Bruker).

For the tensile test, the dog-bone-shaped tensile specimens with a gauge length of 10 mm were machined from the post-treatment processed sheets by electrical discharge machining (EDM), and the length direction of the specimen was consistent with the rolling direction. The oxidation layer formed during EDM cutting was removed by mechanical grinding, using SiC paper. Both sides of the specimens were also ground resulting in a final thickness of ~2.0 mm and a gauge width of ~2.1 mm. Ultimate tensile tests were carried out by an electronic universal material testing machine (Instron 5967, Boston, MA, USA) at an initial strain rate of 10^{-3} s^{-1}. The strain evolution during the tensile test was measured by an AVE camera. More than three samples were tested to confirm reproducibility.

3. Results and Discussion

Figure 1 shows the microstructure of N0 and N0.3 HEAs after annealing at 800 °C for 1 h. The N0 HEA (Figure 1a) exhibits a fully recrystallized microstructure with an average equiaxed grain size of about 22 μm. Meanwhile, the N0.3 HEA (Figure 1b) exhibits a partially recrystallized microstructure with large-sized grains elongated along the rolling direction and small-sized equiaxed grains distributed along the shear deformed zone. The XRD traces in Figure 1c show that as-annealed N0 and N0.3 HEAs are FCC single-phase, without phase transformation during cold-rolling and annealing processes. In detail, as shown in magnified XRD traces of Figure 1d, the FCC peaks of N0.3 HEA shifted slightly to

a lower angle compared with those of N0 HEA. Table 1 summarizes the (111) peak position and lattice parameter of as-annealed N0 and N0.3 HEAs. According to the Bragg's formula, we have the following:

$$2d \sin \theta = n\lambda \tag{1}$$

where d is crystal plane spacing, θ is diffraction angel, and λ is the wavelength. The diffraction peak will shift to a lower angle with the increase of the distance d between the crystal planes. The interstitial N can induce lattice distortion, which is closely related to larger d-spacing. Therefore, the XRD peak positions of N0.3 HEA shift to a lower angle. Additionally, as shown in Figure 1c, the (220) peak abnormally exhibits the highest intensity comparing with other peaks of FCC phase in as-annealed N0.3 HEA. This should be related to (crystallographic) texture in non-recrystallized microstructure, which is presented in detail in the following figures.
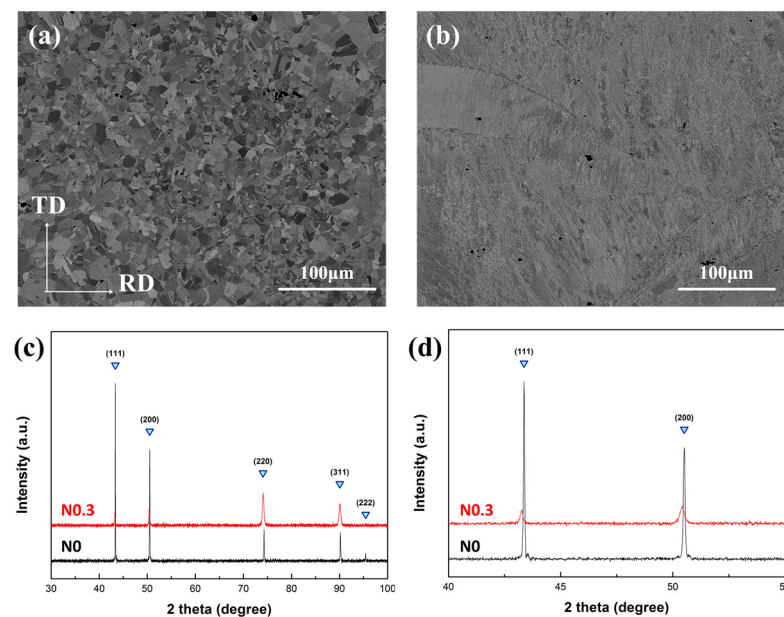

Figure 1. Microstructure and XRD patterns of as-annealed N0 and N0.3 HEAs: (**a**) BSE image of N0 HEA; (**b**) BSE image of N0.3 HEA; (**c**) XRD patterns of N0 and N0.3 HEAs obtained in the range of 30° to 100°; (**d**) XRD patterns of N0 and N0.3 HEAs obtained in the range of 40° to 55°.

Table 1. Peak position (111) and lattice constant of as-annealed N0 and N0.3 HEAs.

Alloy	2θ (°)	Lattice Constant (Å)
N0	43.36926	3.610846
N0.3	43.26820	3.618874

Figure 2 shows the EBSD results of as-annealed N0.3 HEA, which can further reveal the detailed microstructure. The phase map in Figure 2a shows that N0.3 HEA exhibits a single-phase FCC structure (red color). In other words, the addition of nitrogen does not change the main phase constitution of CoCrFeMnNi HEA under post-processing conditions in this study. Combined with the grain map (Figure 2b) and the grain distribution map (Figure 2c), the (area-weighted) volume fraction of recrystallized and non-recrystallized zones was measured as ~23% and ~77%, respectively. The average grain size of recrystallized zones is about ~5 μm, which is over 5 times smaller than that of non-recrystallized zones. The position of recrystallized grains corresponds to the shear bands formed during cold-rolling, which means the driving force of recrystallization in the high strain region (shear bands areas) is larger than that in the low strain region under the current post-processing conditions. The kernel average misorientation (KAM) map (Figure 2d) reveals that the density

of geometric dislocation (GND) in elongated large grains is higher than that in equiaxed grains. This confirms that the large-size grains are typical non-recrystallized zones with residual strain via cold-rolling, while the small-size grains are recrystallized regions with complete strain recovery. Furthermore, *z*-axis inverse pole Figure (IPF) (Figure 2e) and *x*-axis IPF (Figure 2f) suggest that {101} <111> and {112} <111> textures remain in the non-recrystallized grains, which may be inherited from the as-rolled HEA.
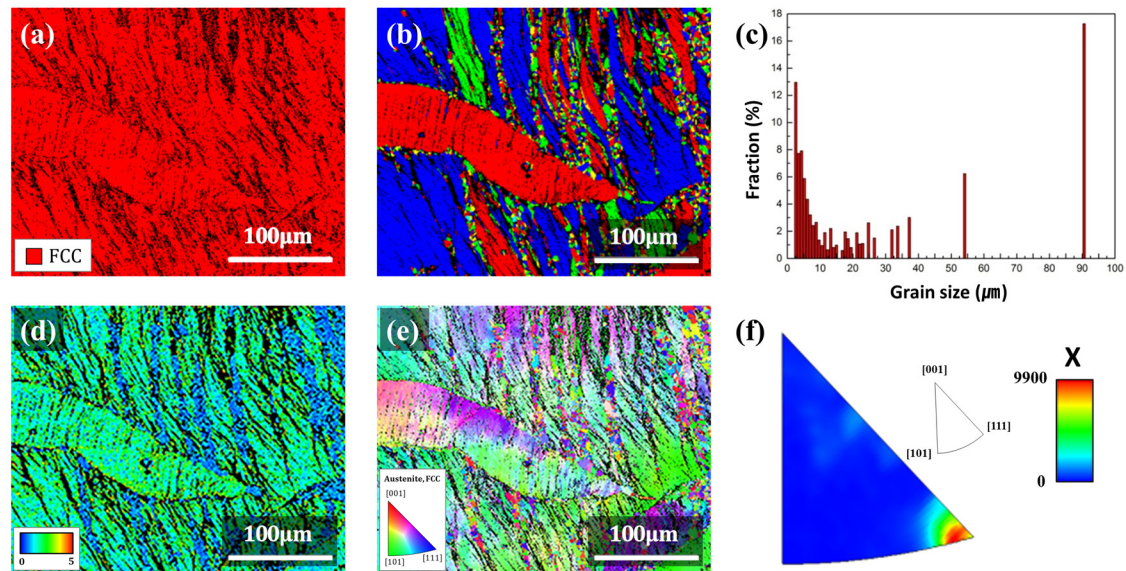

Figure 2. EBSD results of as-annealed N0.3 HEA: (**a**) phase map; (**b**) grain map; (**c**) grain size distribution map; (**d**) KAM map; (**e**) Z-IPF map (color-coded with respect to the *z*-axis orientation); (**f**) color legend for IPF map (color-coded with respect to the *x*-axis orientation).

Figure 3 shows EBSD results of as-rolled N0.3 HEA in order to confirm more clearly the variation of microstructure before and after annealing for recrystallization. The phase map in Figure 3a shows that the as-rolled N0.3 HEA exhibits a single-phase FCC structure without phase transformation under high strained conditions during cold-rolling. However, the KAM map (Figure 3b) suggests the microstructure has irregular strained zones. For example, the upper grain with higher dislocation density in Figure 3b went through more severe deformation compared to the lower grain. Furthermore, IPF maps (Figure 3c,d) reveal the upper grain tends to form {112} <111> texture during cold-rolling, while the lower grain is dominated by {101} <100> texture. This is corresponding to the {101} <100> Goss texture and {112} <111> copper texture of FCC metal after cold-rolling [34]. Compared with the {101} <111> and {112} <111> textures in as-annealed N0.3 HEA (Figure 2), it can be understood that although the large-sized grains do not recrystallize during subsequent annealing for recrystallization in this study, the grain orientation torsion occurs due to thermal action. Consequently, the texture type in the non-recrystallized grains of as-annealed N0.3 HEA is consistent with that of deformed copper texture and slightly different from that of Goss texture.
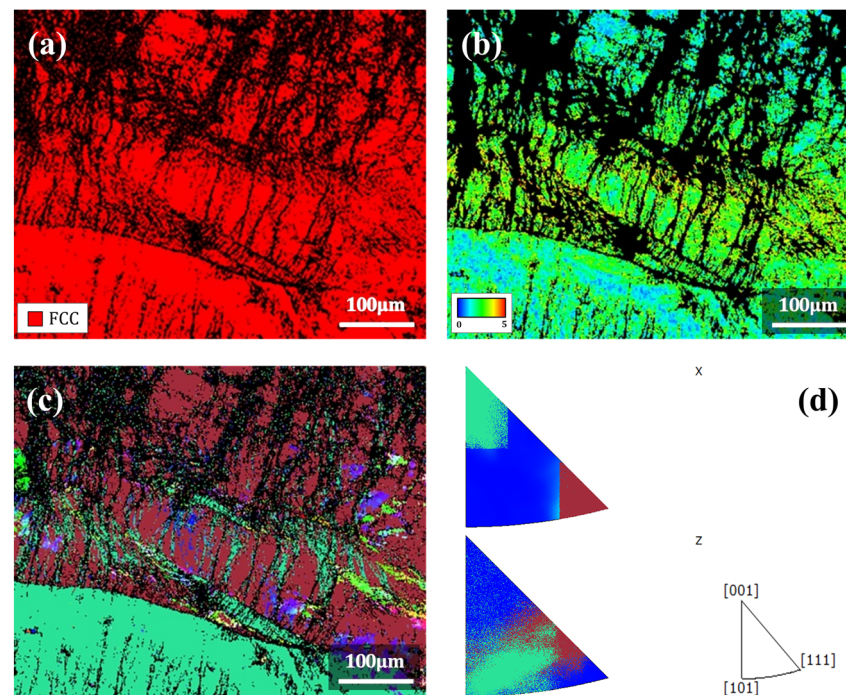
Figure 3. EBSD results of as-rolled N0.3 HEA: (**a**) phase map, (**b**) KAM map, (**c**) Z-IPF map, and (**d**) color legends for IPF map (color-coded with respect to the *x*- and *z*-axis orientation).

To check whether the nanoscale second phase is precipitated in the FCC matrix, high magnification FE-SEM images were obtained in as-annealed N0 (not shown) and N0.3 HEA (Figure 4). Although there is no precipitation in as-annealed N0, surprisingly, in as-annealed N0.3, there are plenty of second-phase particles precipitated at the boundaries of parent grains, the boundaries of recrystallized grains, and the interior shear bands of non-recrystallized grains, as shown in Figure 4a,b. The average size of the second-phase particles is about ~300 nm, which is a size that cannot be easily observed through general XRD or normal SEM observation (Figure 1). The results of the EDS line scan in Figure 4c show that the second-phase particles are Cr-enrich nitrides.

Figure 5 is the Kikuchi orientation maps of the matrix and precipitates in the recrystallized N0.3 HEA. The average volume fraction of Cr_2N is 3.78 ± 0.13 vol.%, which is calculated in Figure 5a. Phase maps (Figure 5b,c) show that the Cr-enrich nitride is a hexagonal crystal structure. Research on high nitrogen steel shows that chromium nitride generally exists in two forms: CrN and Cr_2N [35–37]. CrN is a face-centered cubic structure, while Cr_2N is a simple hexagonal structure. In addition, the thermodynamic calculation results reveal that the thermal stability of Cr_2N is higher at 800 °C [35–39]. Therefore, it can be understood that the precipitates in the as-annealed N0.3 HEA are Cr_2N. According to the Kikuchi crystal orientation maps (Figure 5d,e), there are $\{111\}_M \| \{0001\}_P$ and

$<110>_M \| < 1\bar{1}00 >_P$ crystal orientation relationships between Cr_2N and the matrix. For the Cr_2N precipitates in the recrystallization region, it can retard the growth of recrystallized grains and refine the recrystallized grains due to the pinning effect on the grain boundary. When Cr_2N precipitates in the non-recrystallized region, the movement of dislocations can be hindered, which inhibits the occurrence of recrystallization. Therefore, the N-doping in CoCrFeMnNi HEA results in a unique complex heterogeneous microstructure via inhibiting the recrystallization process, allowing grain refinement and precipitating nanoscale Cr_2N particles.
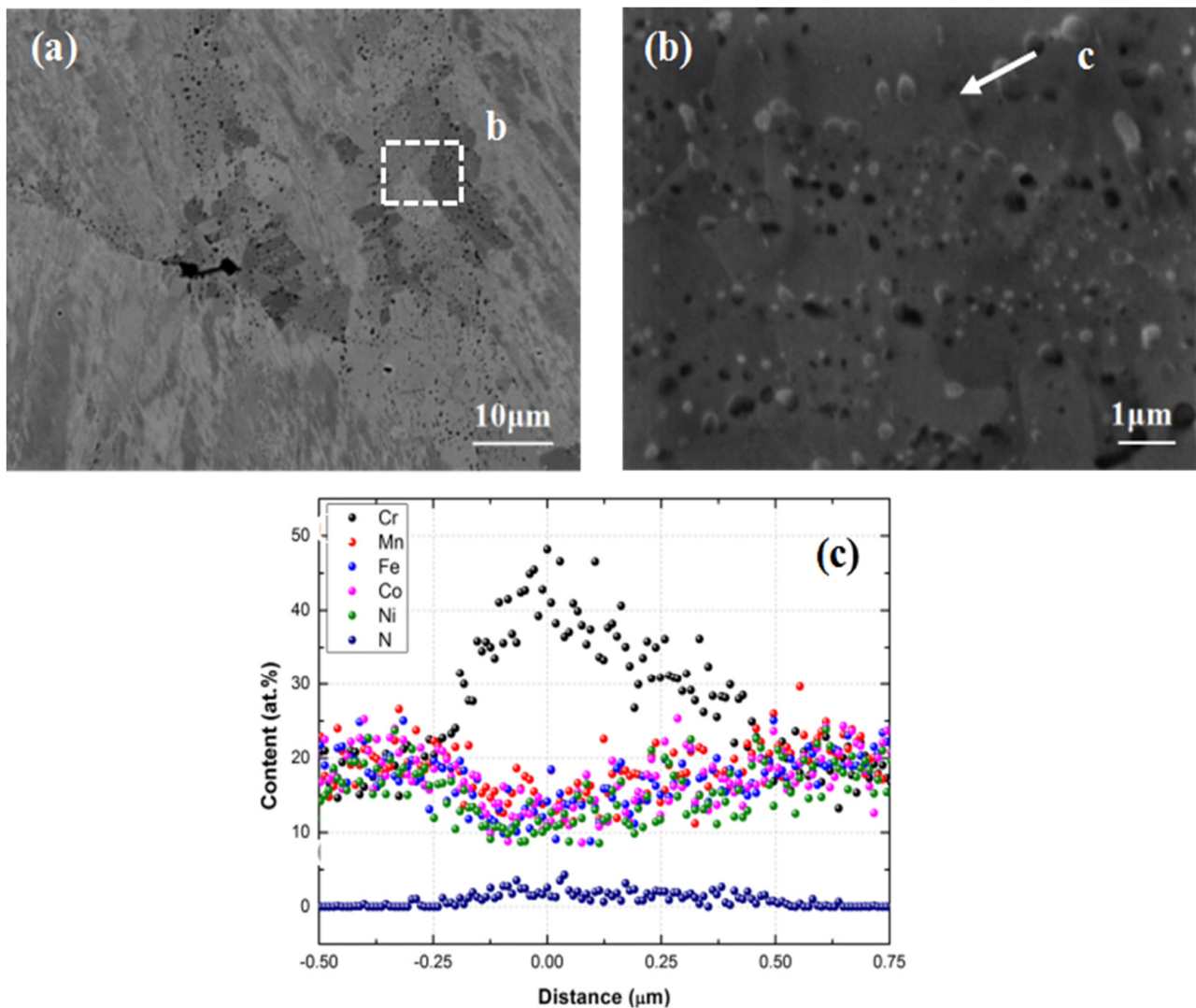
Figure 4. High magnification SEM images and EDS line scan of as-annealed N0.3 HEA: (**a**) BSE image; (**b**) magnified BSE image of b in (**a**); (**c**) EDS line scan of the precipitate c in (**b**).

Figure 6 shows (a) the engineering stress–strain curve at room temperature and (b, c) fractography of as-annealed N0 and N0.3 HEAs. The yield strength significantly increases from 320 MPa in N0 HEA to 690 MPa in N0.3 HEA, and the ultimate tensile strength also increases from 670 MPa in N0 HEA to 940 MPa in N0.3 HEA. However, the elongation decreases from 40% in N0 HEA to 10% in N0.3 HEA according to the strength–ductility trade-off relationship. The fractography of N0 HEA (Figure 6b) shows a dimple feature, while that of N0.3 HEA (Figure 6c) shows a tearing edge feature. This result means that the addition of nitrogen in CoCrFeMnNi HEA changes the deformation mode from ductile fracture to brittle fracture under the identical post-processing condition.
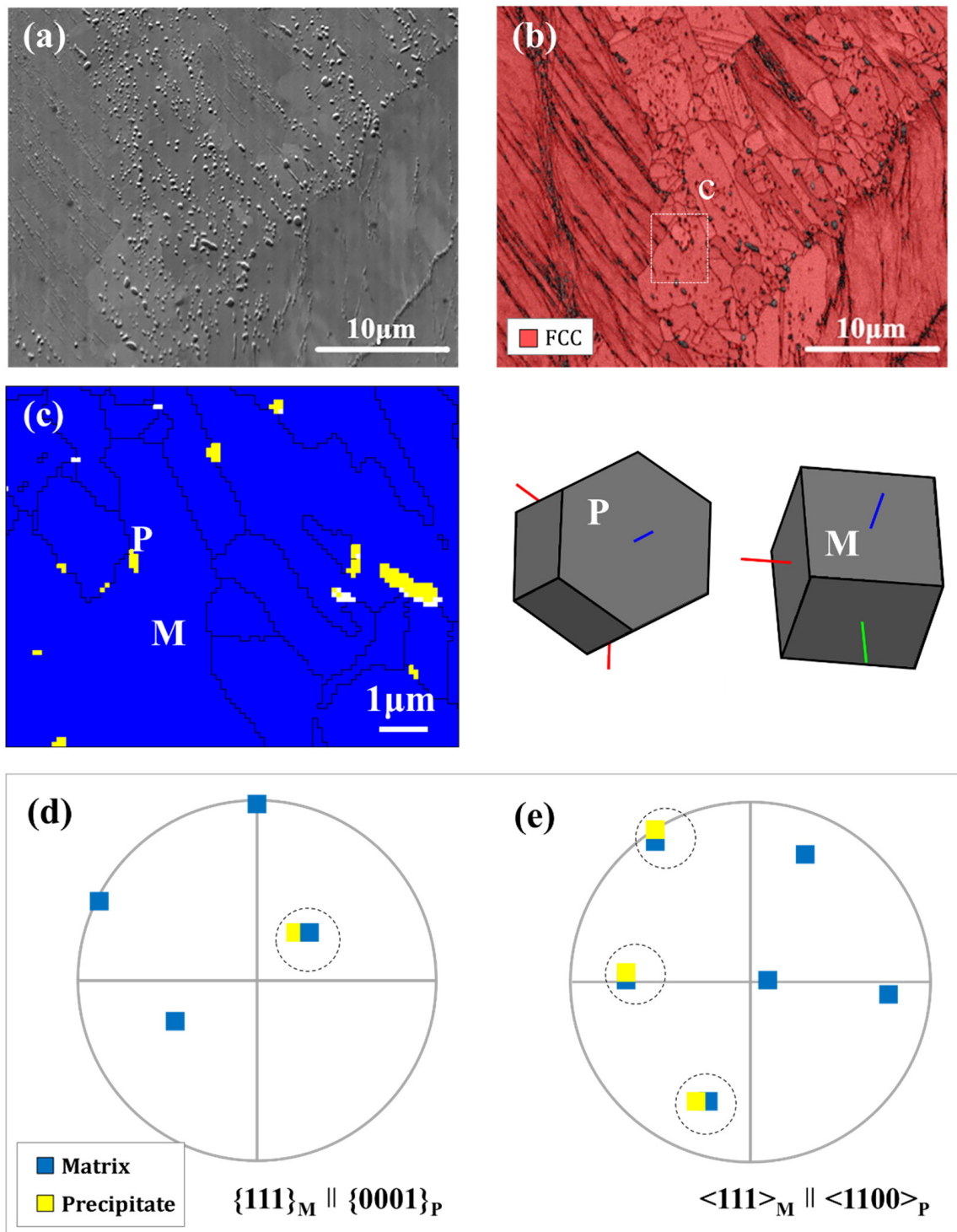
Figure 5. Kikuchi orientation relationship between matrix and the precipitate in as-annealed N0.3 HEA: (**a**) BSE image; (**b**) phase map; (**c**) phase map of c in (**b**); (**d**) Kikuchi orientation relationship in the $\{111\}_M\|\{0001\}_P$ plane; (**e**) Kikuchi orientation relationship in the $<110>_M\|<1\bar{1}00>_P$ direction.

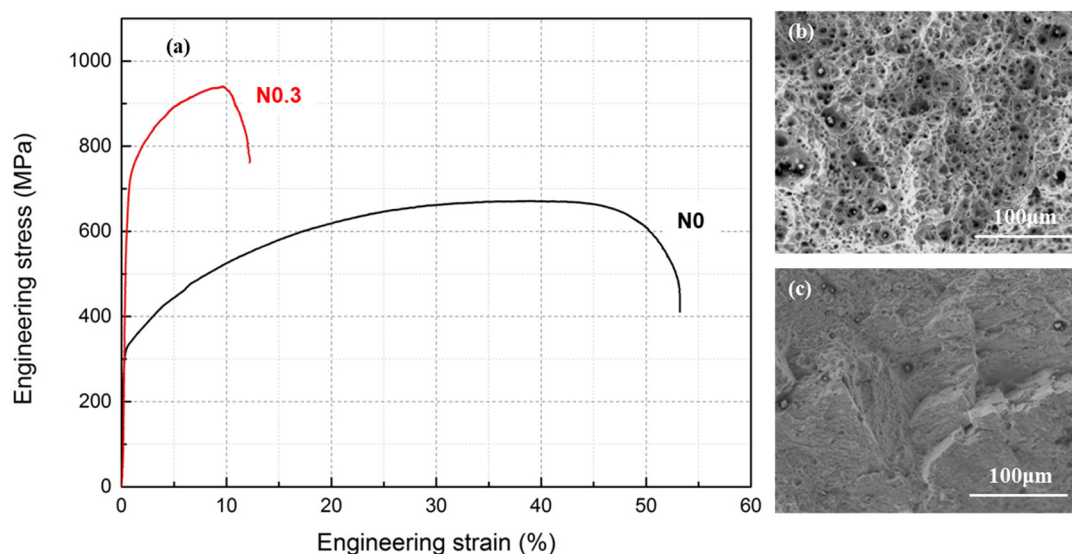**Figure 6.** (**a**) Engineering stress–strain curves and (**b**,**c**) fractography of an-annealed N0 and N0.3 HEAs.

In general, the main strengthening mechanism in alloys can be classified into dislocation strengthening ($\Delta\sigma_D$), precipitation strengthening ($\Delta\sigma_P$), grain refinement strengthening ($\Delta\sigma_G$), solid solution strengthening ($\Delta\sigma_S$), phase transformation strengthening ($\Delta\sigma_{PT}$), etc. Herein, according to the microstructure evolution, the strengthening mechanism of the complex heterogeneous microstructure induced by nitrogen in CoCrFeMnNi HEA can be analyzed as follows:

$$\Delta\sigma_y = \Delta\sigma_D + \Delta\sigma_G + \Delta\sigma_S + \Delta\sigma_P \tag{2}$$

In detail, first, the EBSD KAM map in Figure 2d shows that the high-density dislocations in non-recrystallized grains of as-annealed N0.3 HEA are retained, which can result in a dislocation strengthening ($\Delta\sigma_D$). A Bailey–Hirsch formula is applied to calculate the relationship as follows [40]:

$$\Delta\sigma_D = M\alpha Gb\rho^{1/2} \tag{3}$$

where α is a constant for fcc metals, M is the Taylor factor, G is the shear modulus, b is the Burgers vector, and ρ is the dislocation density. Here, $\alpha = 0.2$, $M = 3.06$ [30], and $b = 0.255$ nm. G is assumed as 80 GPa (the average value of reported FCC HEAs, 76.2 ± 8.15 [39]). The average dislocation density of N0.3 HEA with partially recrystallized microstructure is estimated to be around $10^{14}/m^2$ [31]. Therefore, the value of the dislocation strengthening ($\Delta\sigma_D$) in as-annealed N0.3 HEA is calculated as 124.8 MPa.

Second, the EBSD grain map in Figure 2b and grain size distribution map in Figure 2c suggest that the recrystallized grains in as-annealed N0.3 HEA exhibit a relatively smaller grain size down to about 5 μm. This may attribute to the dislocation pinning effect of precipitation on the grain boundaries, which can result in grain refinement strengthening ($\Delta\sigma_G$). Accordingly, yield strength increment caused by grain size difference can be expressed as based on the Hall–Petch relationship [6]:

$$\Delta\sigma_G = k_y\left(d_{N0.3}^{-1/2} - d_{N0}^{-1/2}\right) \tag{4}$$

where k_y is the strengthening coefficient, and $d_{N0.3}$ and d_{N0} represent the average grain size of the N0.3 and N0 HEA, respectively. Here, the k_y value adopted in the present study is 494 MPa·μm$^{1/2}$ of Cantor HEA [6]; $d_{N0.3}$ and d_{N0} are 5 and 22 μm, respectively. Moreover, since $\Delta\sigma_G$ might be related to only the recrystallized grain, the value obtained with Equation (4) is multiplied by the fraction of fully recrystallized grains in as-annealed N0.3 HEA, ~23%. Indeed, the value of grain refinement strengthening ($\Delta\sigma_G$) in as-annealed N0.3 HEA is calculated as 26.6 MPa.

Third, XRD patterns (Figure 1c) show some solutionized nitrogen in the matrix of as-annealed N0.3 HEA, resulting in interstitial solid solution strengthening ($\Delta\sigma_S$). Ignoring the influence of Cr_2N precipitation on the N content in the matrix, the estimated strengthening coefficient of N-doped CrMnFeCoNi HEA is ~124 MPa/at.% (cited by the nitrogen austenitic steels [35]. Since the nitride precipitation is formed, we can assume that the matrix of N0.3 HEA has solute nitrogen atoms as maximum solubility. The maximum solubility of nitrogen in Cantor HEA is reported as 0.18 wt.% (~0.72 at.%) [41]. Therefore, the $\Delta\sigma_S$ without the effect of precipitation can be calculated as ~89.3 MPa.

Finally, SEM and EBSD results in Figures 4 and 5 reveal that the nanoscale Cr_2N particles precipitate in as-annealed N0.3 alloy, which can result in an Orowan strengthening effect ($\Delta\sigma_P$) due to dislocation bowing around particles in the as-annealed N0.3 HEA with the complex heterogeneous microstructure. Combining the above values of $\Delta\sigma_D$, $\Delta\sigma_G$, and $\Delta\sigma_S$ and using Equation (2), the value of precipitation strengthening ($\Delta\sigma_P$) in as-annealed N0.3 HEA is calculated as ~129.3 MPa.

Based on the discussion above, the contribution of independent strengthening mechanisms can be roughly sequenced as precipitation strengthening ($\Delta\sigma_P$) $\geq$ dislocation strengthening ($\Delta\sigma_D$) > interstitial solid solution strengthening ($\Delta\sigma_P$) > grain refinement strengthening ($\Delta\sigma_G$); however, some coefficients should be updated through deeper investigations, such as the solid solution coefficient due to the intrinsic properties of HEAs, and the strengthening coefficient of Hall–Petch relationship [42–44] due to potential short-range orders (SROs) influenced by the doped nitrogen in HEAs. Consequently, the exceptional strengthening in as-annealed N0.3 HEA can be achieved by the simultaneous operation of various strengthening mechanisms from the complex heterogeneous microstructure. Although we have not yet solved the problem of ductility reduction as the strength increases because the microstructure optimization is not yet complete in this study, there is a promising possibility to overcome the strength–ductility trade-off in the N-doped HEAs due to their unique complex heterogeneous microstructure through the precise control of the N contents or the post-processing conditions, which will merit further investigation.

4. Conclusions

In the present study, we carefully investigate the effect of N doping in the equiatomic CoCrFeMnNi HEA on the microstructure evolution and mechanical properties under the same post-processing conditions (homogenization (1100 °C for 20 h), cold-rolling (reduction ratio of 60%), and subsequent annealing (800 °C for 1 h)). The main conclusions are as follows:

1. N doping in the CoCrFeMnNi HEA results in a unique complex heterogeneous microstructure via inhibiting the recrystallization process, allowing grain refinement, and precipitating nanoscale Cr_2N particles, simultaneously.
2. The yield strength and ultimate tensile strength of as-annealed N0.3 HEA are 690 and 940 MPa, respectively, which exceeds more than twice those of as-annealed N0 HEA. Although the elongation of as-annealed N0.3 HEA (~10%) is much lower than that of as-annealed N0 HEA (~40%), it still has a meaningful value that can be used commercially.
3. The exceptional strengthening in as-annealed N0.3 HEA can be achieved by the simultaneous operation of four different strengthening mechanisms from the unique complex heterogeneous microstructure. The contribution of different strengthening mechanisms to the overall yield strength increment in N0.3 HEA is~129.3 MPa of $\Delta\sigma_P$ $\geq$ ~124.8 MPa of $\Delta\sigma_D$ > ~89.3 MPa of $\Delta\sigma_S$ > ~26.6 MPa of $\Delta\sigma_G$, which means that yield-strength increment in as-annealed N0.3 HEA is attributed to the combination effect of the precipitation of Cr_2N, dislocation strengthening (via 77% non-recrystallized zone with higher dislocation density), and the solid solution of nitrogen (via a large amount of solution-soluted N content, 0.3 wt.%).

Although it has not been fully elucidated how to overcome the strength–ductility trade-off relationship, it is expected that precise control of the unique complex heterogeneous structure of N-doped FCC HEA will pave the way for overcoming one of the oldest dilemmas of structural materials, strength–ductility trade-off, just as composites can create unique properties.

Author Contributions: Conceptualization, J.Z., K.N.Y., E.S.P.; Methodology, J.Z.; Sample preparation, J.Z., M.S.K.; Microstructure analysis, J.Z., H.S.A., J.Y.K.; Writing—review and editing, J.Z., K.N.Y., W.H.R., E.S.P.; supervision, E.S.P. All authors have read and agreed to the published version of the manuscript.

Data Availability Statement: Not applicable.

Conflicts of Interest: The authors declare no conflict of interest.

References

1. Zhang, Y.; Zuo, T.T.; Tang, Z.; Gao, M.C.; Dahmen, K.A.; Liaw, P.K.; Lu, Z.P. Microstructures and properties of HEAs. *Prog. Mater. Sci.* **2014**, *61*, 1–93. [CrossRef]
2. Tsai, M.H.; Yeh, J.W. HEAs: A critical review. *Mater. Res. Lett.* **2014**, *2*, 107–123. [CrossRef]
3. Miracle, D.B.; Senkov, O.N. A critical review of high entropy alloys and related concepts. *Acta Mater.* **2017**, *122*, 448–511. [CrossRef]
4. Choi, Y.T.; Bae, J.W.; Park, J.M.; Lee, H.H.; Kwon, H.S.; Son, S.J.; Ahn, D.H.; Kim, H.S. Stretch-flangeability of CoCrFeMnNi HEA. *Mater. Sci. Eng. A* **2021**, *841*, 141241. [CrossRef]
5. Guo, S.; Chen, H.; Wang, M. Research on the dislocation differences of CoCrFeMnNi with different local chemical orders during room temperature tensile test. *J. Alloys Compd.* **2021**, *868*, 159215. [CrossRef]
6. Otto, F.; Dlouhý, A.; Somsen, C.; Eggeler, H.B.; George, E.P. The influences of temperature and microstructure on the tensile properties of a CoCrFeMnNi HEA. *Acta Mater.* **2013**, *61*, 5743–5755. [CrossRef]
7. Gludovatz, B.; Hohenwarter, A.; Catoor, D.; Chang, E.H.; George, E.P.; Ritchie, R.O. A fracture-resistant HEA for cryogenic applications. *Science* **2014**, *345*, 1153–1158. [CrossRef] [PubMed]
8. Naeem, M.; He, H.Y.; Zhang, F.; Naeem, M.; He, H.Y.; Zhang, F.; Huang, H.L.; Harjo, S.; Kawasaki, T.; Wang, B.; et al. Cooperative deformation in HEAs at ultralow temperatures. *Sci. Adv.* **2020**, *6*, eaax4002. [CrossRef]
9. Senkov, O.; Isheim, D.; Seidman, D.; Pilchak, A.L. Development of a refractory high entropy superalloy. *Entropy* **2016**, *18*, 102. [CrossRef]
10. Quiambao, K.F.; McDonnell, S.J.; Schreiber, D.K.; Gerard, A.Y.; Freedy, K.M.; Lu, P.; Saal, J.E.; Frankel, G.S.; Scully, J.R. Passivation of a corrosion resistant high entropy alloy in non-oxidizing sulfate solutions. *Acta Mater.* **2019**, *164*, 362–376. [CrossRef]
11. Lei, Z.F.; Liu, X.J.; Wu, Y.; Wang, H.; Jiang, S.H.; Wang, S.D.; Hui, X.D.; Wu, Y.D.; Gault, B.; Kontis, P.; et al. Enhanced strength and ductility in a HEA via ordered oxygen complexes. *Nature* **2018**, *563*, 546–550. [CrossRef] [PubMed]
12. Medina, L.Z.; da Costa, M.V.T.; Paschalidou, E.M.; Lindwall, G.; Riekehr, L.; Korvela, M.; Fritze, S.; Kolozsvári, S.; Gamstedt, E.K.; Nyholm, L.; et al. Enhancing corrosion resistance, hardness, and crack resistance in magnetron sputtered high entropy CoCrFeMnNi coatings by adding carbon. *Mater. Des.* **2021**, *205*, 109711. [CrossRef]
13. Yang, T.; Zhao, Y.L.; Tong, Y.; Jiao, Z.B.; Wei, J.; Cai, J.X.; Han, X.D.; Chen, D.; Hu, A.; Kai, J.J.; et al. Multicomponent intermetallic nanoparticles and superb mechanical behaviors of complex alloys. *Science* **2018**, *362*, 933–937. [CrossRef]
14. Gao, X.Z.; Lu, Y.P.; Zhang, B.; Liang, N.N.; Wu, G.Z.; Sha, G.; Liu, J.Z.; Zhao, Y.H. Microstructural origins of high strength and high ductility in an AlCoCrFeNi$_{2.1}$ eutectic HEA. *Acta Mater.* **2017**, *141*, 59–66. [CrossRef]
15. Wu, Q.F.; Wang, Z.J.; Hu, X.B.; Zheng, T.; Yang, Z.; He, F.; Li, J.; Wang, J. Uncovering the eutectics design by machine learning in the Al-Co-Cr-Fe-Ni high entropy system. *Acta Mater.* **2020**, *182*, 278–286. [CrossRef]
16. Han, Y.; Li, H.B.; Feng, H.; Tian, Y.Z.; Jiang, Z.H.; He, T. Mechanism of dislocation evolution during plastic deformation of nitrogen-doped CoCrFeMnNi HEA. *Mater. Sci. Eng. A* **2021**, *814*, 141235. [CrossRef]
17. Wang, Z.W.; Baker, I.; Cai, Z.H.; Chen, S.; Poplawsky, J.D.; Guo, W. The effect of interstitial carbon on the mechanical properties and dislocation substructure evolution in Fe$_{40.4}$Ni$_{11.3}$Mn$_{34.8}$Al$_{7.5}$Cr$_6$ high entropy alloys. *Acta Mater.* **2016**, *120*, 228–239. [CrossRef]
18. Seol, J.B.; Bae, J.W.; Li, Z.M.; Han, J.C.; Kim, J.G.; Raabe, D.; Kim, H.S. Boron doped ultra-strong and ductile HEAs. *Acta Mater.* **2018**, *151*, 366–376. [CrossRef]

19. Xie, Y.C.; Cheng, H.; Tang, Q.H.; Chen, W.; Chen, W.K.; Dai, P.Q. Effects of N addition on microstructure and mechanical properties of CoCrFeNiMn high entropy alloy produced by mechanical alloying and vacuum hot pressing sintering. *Intermetallics* **2018**, *93*, 228–234. [CrossRef]

20. Klimova, M.; Shaysultanov, D.; Semenyuk, A.; Zherebtsov, S.; Salishchev, G.; Stepanov, N. Effect of nitrogen on mechanical properties of CoCrFeMnNi high entropy alloy at room and cryogenic temperatures. *J. Alloys Compd.* **2020**, *849*, 156633. [CrossRef]

21. Jodi, D.E.; Park, J.Y.; Park, N.E. Strengthening of ultrafine-grained equiatomic CoCrFeMnNi HEA by nitrogen addition. *Mater. Lett.* **2020**, *258*, 126772. [CrossRef]

22. Xiong, F.; Fu, R.; Li, Y.; Xu, B.; Qi, X. Influences of nitrogen alloying on microstructural evolution and tensile properties of CoCrFeMnNi HEA treated by cold-rolling and subsequent annealing. *Mater. Sci. Eng. A* **2020**, *787*, 139472. [CrossRef]

23. Sathiyamoorthi, P.; Kim, H.S. High-entropy alloys with heterogeneous microstructure: Processing and mechanical properties. *Prog. Mater. Sci.* **2020**, 100709. [CrossRef]

24. Ma, E.; Zhu, T. Towards strength–ductility synergy through the design of heterogeneous nanostructures in metals. *Mater. Today* **2017**, *20*, 323–331. [CrossRef]

25. Huang, C.X.; Wang, Y.F.; Ma, X.L.; Yin, S.; Höppel, H.W.; Göken, M.; Wu, X.L.; Gao, H.J.; Zhu, Y.T. Interface affected zone for optimal strength and ductility in heterogeneous laminate. *Mater. Today* **2018**, *21*, 713–719. [CrossRef]

26. Li, Z.M.; Pradeep, K.G.; Deng, Y.; Raabe, D.; Tasan, C.C. Metastable high-entropy dual-phase alloys overcome the strength–ductility trade-off. *Nature* **2016**, *534*, 227–230. [CrossRef] [PubMed]

27. YJo, H.; Jung, S.; Choi, W.M.; Sohn, S.S.; Kim, H.S.; Lee, B.J.; Kim, N.J.; Lee, S. Cryogenic strength improvement by utilizing room-temperature deformation twinning in a partially recrystallized VCrMnFeCoNi HEA. *Nat. Commun.* **2017**, *8*, 15719.

28. Wu, X.L.; Zhu, Y.T. Heterogeneous materials: A new class of materials with unprecedented mechanical properties. *Mater. Res. Lett.* **2017**, *5*, 527–532. [CrossRef]

29. Kim, S.H.; Kim, H.; Kim, N.J. Brittle intermetallic compound makes ultrastrong low-density steel with large ductility. *Nature* **2015**, *518*, 77–79. [CrossRef]

30. Kocks, U.F. A Statistical Theory of Flow Stress and Work-hardening. *Philos. Mag.* **1965**, *123*, 541–566. [CrossRef]

31. Wu, S.W.; Wang, G.; Wang, Q.; Zhang, T.Y. Enhancement of strength-ductility trade-off in a HEA through a heterogeneous structure. *Acta Mater.* **2019**, *165*, 444–458. [CrossRef]

32. Li, Z.M. Interstitial equiatomic CoCrFeMnNi HEAs: Carbon content, microstructure, and compositional homogeneity effects on deformation behavior. *Acta Mater.* **2019**, *164*, 400–412. [CrossRef]

33. Semenyuk, A.; Klimova, M.; Shaysultanov, D.; Salishchev, G.; Zherebtsov, S.; Stepanov, N. Effect of nitrogen on microstructure and mechanical properties of the CoCrFeMnNi high-entropy alloy after cold rolling and subsequent annealing. *J. Alloys Compd.* **2021**, *888*, 161452. [CrossRef]

34. ASTM E112. *Standard Test Methods for Determining Average Grain Size*; American Society for Testing and Materials: West Conshohocken, PA, USA, 1996.

35. Gavriljuk, V.G.; Berns, H. *High Nitrogen Steels*, 1st ed.; Springer: New York, NY, USA, 1999.

36. Yong, Q.L. *Secondary Phases in Steels*, 1st ed.; Metallurgical Industry Press: Beijing, China, 2006.

37. Kikuchi, M.; Kajihara, M.; Choi, S.K. Cellular precipitation involving both substitutional and interstitial solutes: Cellular precipitation of Cr_2N in Cr-Ni austenitic steels. *Mater. Sci. Eng. A* **1991**, *146*, 131–150. [CrossRef]

38. Rayaprolu, D.B.; Hendry, A. Cellular precipitation in a nitrogen alloyed stainless steel. *Mater. Sci. Technol.* **1989**, *5*, 328–332. [CrossRef]

39. Ono-Nakazato, H.; Taguchi, K.; Usui, T.; Tamura, K.; Tomatsu, Y. Determination of standard Gibbs energies of formation of Cr_2N and CrN. *Metall. Mater. Trans. B* **2001**, *32*, 1113–1118. [CrossRef]

40. Courtney, T.H. *Mechanical Behavior of Materials*; Long Grove Press: Waveland, MI, USA, 2005.

41. Traversier, M.; Mestre-Rinn, P.; Peillon, N.; Rigal, E.; Boulnat, X.; Tancret, F.; Dhers, J.; Fraczkiewic, A. Nitrogen-induced hardening in an austenitic CrFeMnNi high-entropy alloy (HEA). *Mater. Sci. Eng. A* **2021**, *804*, 14072. [CrossRef]

42. Ding, Q.Q.; Zhang, Y.; Chen, X.; Fu, X.Q.; Chen, D.K.; Chen, S.J.; Gu, L.; Wei, F.; Bei, H.B.; Gao, Y.F.; et al. Tuning element distribution, structure and properties by composition in high-entropy alloys. *Nature* **2019**, *574*, 223–227. [CrossRef]

43. Zhang, R.P.; Zhao, S.T.; Ding, J.; Chong, Y.; Jia, T.; Ophus, C.; Asta, M.; Ritchie, R.O.; Minor, A.M. Short-range order and its impact on the CrCoNi medium-entropy alloy. *Nature* **2020**, *581*, 283–287. [CrossRef] [PubMed]

44. Moravcik, I.; Hadraba, H.; Li, L.L.; Dlouhy, I.; Raabe, D.; Li, Z.M. Yield strength increase of a CoCrNi medium entropy alloy by interstitial nitrogen doping at maintained ductility. *Scr. Mater.* **2020**, *178*, 391–397. [CrossRef]